

Human Insights Driven Latent Space for Different Driving Perspectives: A Unified Encoder for Efficient Multi-Task Inference

Huy-Dung Nguyen¹, Anass Bairouk¹, Mirjana Maras¹, Wei Xiao², Tsun-Hsuan Wang², Patrick Chareyre¹, Ramin Hasani², Marc Blanchon¹, Daniela Rus²

Abstract—Autonomous driving holds great potential to transform road safety and traffic efficiency by minimizing human error and reducing congestion. A key challenge in realizing this potential is the accurate estimation of steering angles, which is essential for effective vehicle navigation and control. Recent breakthroughs in deep learning have made it possible to estimate steering angles directly from raw camera inputs. However, the limited available navigation data can hinder optimal feature learning, impacting the system’s performance in complex driving scenarios. In this paper, we propose a shared encoder trained on multiple computer vision tasks critical for urban navigation, such as depth, pose, and 3D scene flow estimation, as well as semantic, instance, panoptic, and motion segmentation. By incorporating diverse visual information used by humans during navigation, this unified encoder might enhance steering angle estimation. To achieve effective multi-task learning within a single encoder, we introduce a multi-scale feature network for pose estimation to improve depth learning. Additionally, we employ knowledge distillation from a multi-backbone model pretrained on these navigation tasks to stabilize training and boost performance. Our findings demonstrate that a shared backbone trained on diverse visual tasks is capable of providing overall perception capabilities. While our performance in steering angle estimation is comparable to existing methods, the integration of human-like perception through multi-task learning holds significant potential for advancing autonomous driving systems. More details and the pretrained model are available at <https://hi-computervision.github.io/uni-encoder/>.

I. INTRODUCTION

The development of autonomous driving capabilities requires comprehensive understanding, reliable real-time decision-making, and robust control. Traditional approaches to tasks like steering control rely on modular architectures that separate perception, decision-making, and control, each requiring domain-specific expertise and extensive calibration to function effectively [1]. However, recent advancements in deep learning have introduced end-to-end systems, where neural networks directly learn steering commands from raw input data, greatly simplifying the design and reducing the need for manual tuning [2], [3], [4], [5].

Most deep learning-based steering estimation uses Convolutional Neural Networks (CNN) to extract features from RGB images [6], [7], [8], [9], [10]. While these methods demonstrate that CNNs can extract useful information for estimating the steering angle, the training datasets may lack

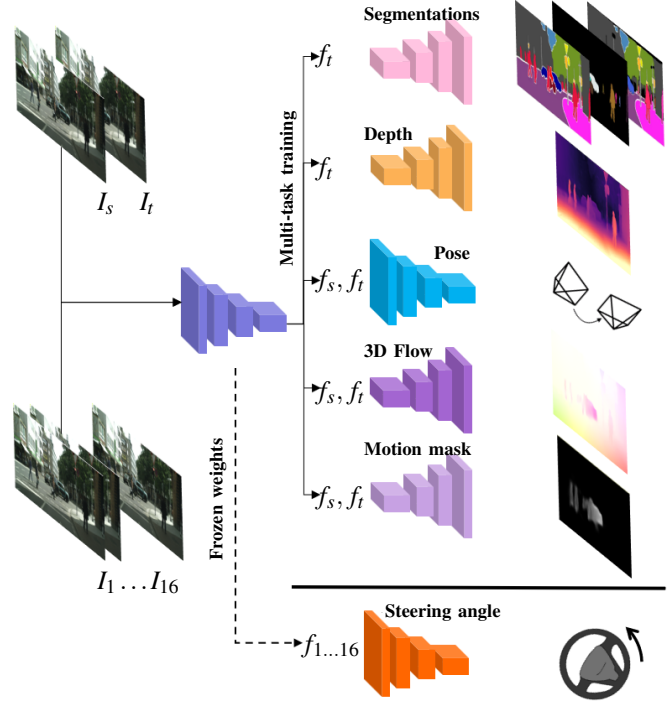


Fig. 1: Our multi-task training strategy. I_s , I_t , $I_{1..16}$ represent the source, target, and 16 sequential images, respectively. Their features, denoted as f_s , f_t , $f_{1..16}$, are extracted (and concatenated when necessary) using our single encoder.

sufficient task-specific details for comprehensive learning. Indeed, Capito *et al.* [11] demonstrate that using optical flow from the same RGB images as an additional input can significantly enhance the original method. This finding raises questions about the scene information encoded by the encoder and whether it effectively captures human-like visual perception needed for navigation.

In this paper, we propose a new approach that integrates human-like perceptual information into a single encoder through a multi-task training strategy. The computer vision tasks we focus on are crucial for urban navigation, including depth, pose and 3D scene flow estimation, as well as semantic, instance, panoptic, and motion segmentation (see Figure 1). Our method offers several key advantages. First, after the initial training, the model can generate multiple outputs with a single pass through the shared encoder, reducing inference time. Additionally, our experimental results demonstrate that this approach yields competitive performance compared to

*This work was supported by Capgemini Engineering.

¹Hybrid Intelligence part of Capgemini Engineering
{first_name.last_name}@capgemini.com

²Computer Science and Artificial Intelligence Lab, Massachusetts Institute of Technology {weixy,tsunw,hasani,rus}@mit.edu

state-of-the-art methods for each individual task. Finally, the encoder model can be frozen and stacked with a prediction head for steering estimation, allowing us to evaluate the relevance of the learned features for this navigation task.

Training this model presents challenges in ensuring it performs well across all tasks. Naively training a shared encoder for depth and pose estimation led to drop in depth accuracy due to inaccurate pose estimation. Moreover, the lack of a comprehensive dataset with labeled data for all tasks led us to use a mixed training approach that combines supervised and self-supervised learning. However, this approach introduced its own issue: tasks with stronger training signals dominated the gradients in the encoder, overshadowing others. For instance, when training segmentation tasks (supervised learning) alongside 3D scene flow and motion mask tasks (self-supervised learning), the latter two struggled to learn effectively. Since these self-supervised tasks are critical for depth estimation in dynamic scenes, this training dominance destabilized the entire self-supervised training process. To this end, the contributions of this paper are:

- A novel pose decoder architecture that leverages the multi-scale features from our shared encoder to enhance depth estimation.
- A strategy to stabilize training by distilling knowledge from a multi-encoder teacher pretrained on same tasks.
- An evaluation of whether a shared encoder trained on multiple tasks can improve steering angle estimation.

II. RELATED WORKS

A. Image segmentation

Image segmentation involves separating an image into segments, grouping pixels by specific criteria. Semantic segmentation assigns pixels to broad classes like roads and buildings, while instance segmentation focuses on distinct objects like cars and people [12]. Traditionally, these tasks were handled separately. To integrate these approaches, Kirillov *et al.* [13] introduced panoptic segmentation, which organizes pixels into amorphous background regions ("stuff") and distinct objects ("things"). However, this led to an additional specialized task rather than unifying these two, with performance falling short of state-of-the-art results in dedicated tasks.

Recent methods have proposed unified models for all three tasks showing high performance but still requiring separate training for each. In a significant advancement, Jain *et al.* introduced OneFormer [14], a model that, given an image and a text prompt specifying the task, produces the corresponding segmentation output. Evaluated on several public datasets, OneFormer set new state-of-the-art benchmarks for all three tasks with a single, jointly trained model. In this paper, we use OneFormer decoders to generate the three mentioned segmentation outcomes.

B. Monocular Depth & Pose Estimation

Monocular depth estimation is a task of predicting the depth of a scene from a single 2D image. Unlike stereoscopic methods, which use different viewpoints as input, monocular depth estimation must infer depth from just one, making it

particularly challenging. Traditional methods mostly based on hand-crafted features, which can lead to inaccuracies in complex scenarios [15]. In a first attempt using deep learning, Eigen *et al.* (2014) introduced a CNN-based model to predict depth maps directly from single images, achieving superior results. However, this method requires ground truth for depth, typically obtained with expensive hardware like LiDAR, limiting its practicality. To overcome this, recent research has shifted to unsupervised methods that use the inherent structure of unlabeled images. Notably, Zhou *et al.* [16] and Godard *et al.* [17] proposed unsupervised methods which employ video sequences to simultaneously learn depth and camera motion, reducing the dependency on labeled data and adapting better to dynamic scenes.

However, unsupervised methods often consider the assumption of a static world, which is not true in most real scenarios. To this end, recent advancements have integrated flow (*e.g.*, 2D or 3D) and motion segmentation in addition to depth and pose estimation, enabling better handling of dynamic objects in the scene [18].

C. Scene Flow and Motion Segmentation

Scene flow estimation is similar to depth estimation but in addition, it can capture 3D motion between consecutive images, while motion segmentation identifies dynamic objects. These tasks, when jointly trained with depth and pose estimation, improve depth accuracy [19], [20]. Jiao *et al.*'s EffiScene network [21] trains on these tasks using stereo images, leveraging the shared geometric structure of scene depth and object movement. Recently, Sun *et al.* [18] propose DynamoDepth framework that further improves flexibility with the capacity of training on only video frames.

Building on DynamoDepth, we propose a single encoder model that requires only two images to estimate scene flow and motion segmentation, reducing complexity compared to the three-image requirement in the original method.

D. Steering angle estimation

The two main research directions for steering estimation are model-based and model-free. Model-based methods rely on vehicle dynamics models, while model-free methods leverage data-driven techniques like deep learning. This paper focuses only on the model-free approach. Bojarski *et al.* [8] introduced an end-to-end steering angle estimation using CNN with a single RGB camera input. Capito *et al.* [11] improved the navigation capability by incorporating optical flow into the input. The importance of temporal information has also been highlighted in many works. Indeed, Eraqi *et al.* [22] employed LSTM networks to enhance steering control, while Xu *et al.* [23] combined fully convolutional networks with LSTM and semantic segmentation for improved road condition interpretation. Lechner *et al.* [2] proposed Neural Circuit Policies (NCPs), which provide interpretable decision maps from high-dimensional inputs. These studies indicate that integrating temporal information between frames can improve steering accuracy.

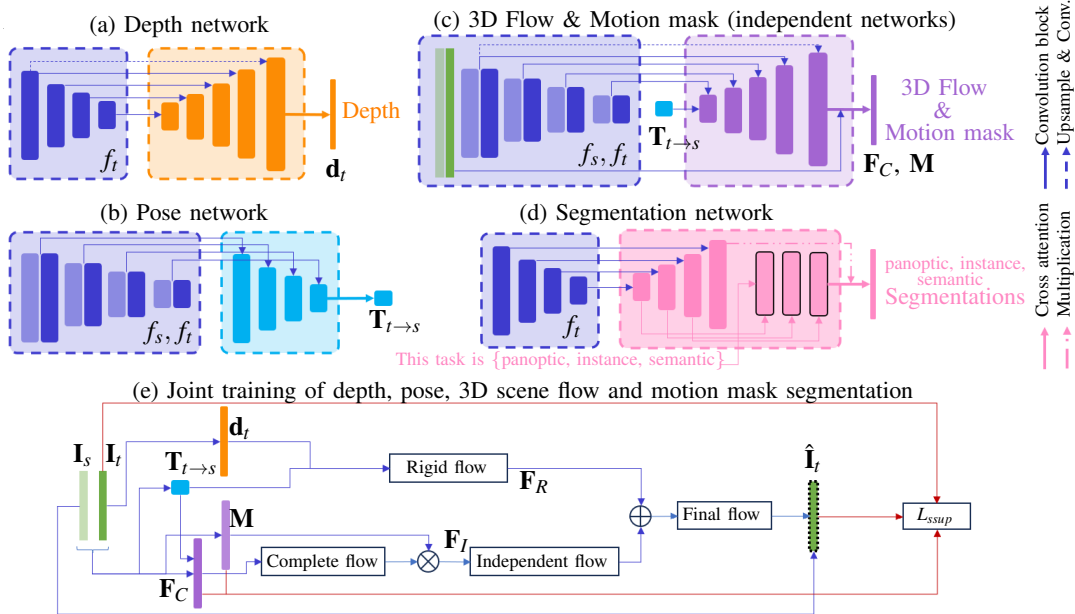


Fig. 2: Simplified architecture of our model: (a) Depth network using target image features f_t to output depth \mathbf{d}_t , (b) Multi-scale pose network using source and target image features f_s, f_t to output relative pose $\mathbf{T}_{t \rightarrow s}$, (c) 3D Scene Flow \mathbf{F}_C and Motion mask \mathbf{M} networks using RGB images and features f_s, f_t , (d) Segmentation network outputting panoptic, instance, and semantic segmentations, and (e) Loss computation L_{sup} for joint training of depth, pose, 3D scene flow, and motion mask segmentation. We denote rigid flow \mathbf{F}_R , independent flow \mathbf{F}_I , final flow, and sampled target image $\hat{\mathbf{I}}_t$.

III. METHODS

Figure 1 illustrates our model architecture, which includes a Swin Tiny encoder [24] and six decoders for: panoptic, instance, and semantic segmentation, depth and pose estimation, 3D scene flow estimation, motion mask segmentation, and steering command prediction. Training was performed in two stages. In the first stage, we pretrained the encoder with five decoders (excluding the steering command decoder) to learn generalized features across tasks. In the second stage, we froze the encoder and added a prediction head for steering estimation to evaluate its performance in navigation.

Due to the lack of a comprehensive dataset with annotations for all tasks, we used the CityScapes dataset [25], which provides high-quality segmentation annotations and a video sequence format suitable for tasks like depth and pose estimation, 3D scene flow, and motion mask segmentation.

A. Panoptic, Instance, and Semantic Segmentations

For these three supervised segmentation tasks, we use the OneFormer approach. This is a task-conditioned universal image segmentation model that achieves state-of-the-art performance across all segmentation tasks with a unified model and architecture. The OneFormer framework adopts a task-conditioned joint training strategy that allows simultaneous training on all segmentation tasks using a single model, reducing resource requirements significantly.

Figure 2d provides a simplified illustration of the OneFormer architecture. This model consists of an encoder and two distinct decoders. The first decoder processes image features to generate all segment-related features. The output from this decoder, along with an embedding of a text prompt

defining the task (e.g., "The task is {panoptic, instance, semantic}"), is then passed to the second decoder. The second decoder uses this information to produce the desired segmentation type. The supervised loss function combines cross-entropy loss for classification, binary cross-entropy for mask predictions, and Dice loss for accurate mask boundary predictions. We trained this model end-to-end on panoptic annotations, from which semantic and instance labels are derived. The overall loss function L_{sup} integrates multiple components to ensure task-specific accuracy:

$$L_{sup} = \lambda_{cls} L_{cls} + \lambda_{bce} L_{bce} + \lambda_{dice} L_{dice} + \lambda_{contrast} L_{contrast}, \quad (1)$$

where:

- L_{cls} is the cross-entropy loss for mask (i.e., region) classification accuracy.
- L_{bce} is the binary cross-entropy loss applied to mask.
- L_{dice} is the Dice loss, helps to improve mask boundaries.
- $L_{contrast}$ is the contrastive loss between object and text queries to make sure the text query is taken into account.

B. Depth, Pose, 3D Flow Estimation, and Motion Mask

For depth estimation, we employ the depth decoder architecture from [26]. In addition, we introduce a novel pose decoder, which is discussed in detail in the next section. For 3D scene flow estimation and motion mask segmentation, we build upon the DynamoDepth approach [18], enhancing it with convolutional blocks including additional non-linearity to increase the model's representational capacity. Concretely, instead of considering the 3D scene flow as a linear combination of the encoder features f and the pose $\mathbf{T}_{t \rightarrow s}$, we consider it as a non linear combination $\mathbf{F}_i = \mathbf{U}(\mathbf{F}_{i+1}) +$

$\text{ConvELU}([a_i, \text{Conv}(a_i)])$ where $a_i = \text{Conv}([\mathbf{U}(\mathbf{F}_{i+1}), f_i])$, $\mathbf{F}_5 = \mathbf{T}_{t \rightarrow s}$, and \mathbf{F} and \mathbf{U} are respectively flow and upscaling operation. By doing this, we increase the complexity of the decoders, which can help the unified encoder to learn simpler and more generalizable features that can effectively support downstream tasks. Figure 2a, b, and c provides simplified illustrations of our networks.

Starting with source \mathbf{I}_s and target frames \mathbf{I}_t , we estimate depth \mathbf{d}_t and relative pose $\mathbf{T}_{t \rightarrow s}$. Using $\mathbf{T}_{t \rightarrow s}$, we calculate 3D rigid flow \mathbf{F}_R . The source and target features are concatenated and passed through the 3D scene flow and motion mask segmentation decoders along with $\mathbf{T}_{t \rightarrow s}$, producing the complete flow \mathbf{F}_C and binary motion mask \mathbf{M} . The independent flow \mathbf{F}_I is computed as $\mathbf{F}_I = \mathbf{M} \times (\mathbf{F}_C - \mathbf{F}_R)$. The final flow $\mathbf{F}_F = \mathbf{F}_R + \mathbf{F}_I$ is used to estimate the target frame $\hat{\mathbf{I}}_t$ from \mathbf{I}_s . The self-supervision loss \mathbf{L}_{ssup} is:

$$\mathbf{L}_{\text{ssup}} = L_{\text{recon}} + L_s + \lambda_c L_c + \lambda_m L_m + \lambda_g L_g, \quad (2)$$

where:

- L_{recon} is the reconstruction loss that combines SSIM and L1 norms weighted by α .
- L_s is the smoothness loss [17] which is a weighted sum of edge-aware smoothness losses for the inverse depth, the \mathbf{F}_C and \mathbf{M} .
- L_c is the motion consistency loss that penalize flow discrepancy $\mathbf{F}_D = \|\mathbf{F}_C - \mathbf{F}_R\|_1$ for static pixels.
- L_m is the motion sparsity loss that penalizes the mask \mathbf{M} with low flow discrepancies using cross-entropy to favor zero motion mask.
- L_g is the above-ground loss that penalizes points projected below the ground plane using RANSAC.

Figure 2e illustrates the data flow for computing the self-supervised loss described above.

C. Towards a Unified Multi-Task Encoder

Unlike the DynamoDepth method, which employs three distinct encoders—one each for depth estimation, pose estimation, and 3D scene flow with motion mask segmentation—we propose a single, unified encoder capable of handling all these tasks, along with three additional segmentation tasks: panoptic, instance, and semantic segmentation. This approach can enhance compactness and efficiency but also introduces several challenges.

The foremost challenge is the shared use of the encoder for both depth and pose estimation tasks, which can compromise depth estimation accuracy due to suboptimal relative pose estimation, as noted in [17]. In the shared encoder approach described in [17], relative pose estimation relies on the concatenated lowest-resolution features from the source and target images. However, these low resolution features can lead to ambiguity in pose estimation between the two images.

To overcome this limitation, we propose a multi-scale pose decoder that leverages multi-scale features from both the source and target images to improve the accuracy of relative pose estimation. Specifically, the images are processed through the shared encoder to extract multi-scale

features. These features are then concatenated (as illustrated in Figure 2b), and convolutional blocks with skip connections are applied to each set of concatenated features, from high to low resolution. Given an input feature f , the output of the convolutional block with skip connections is: $\text{out} = \text{ReLU}(\text{ConvBNReLU}(\text{ConvBN}(f)) + \text{Shortcut}(f))$ where Conv , BN , ReLU refers to the convolution, batch norm layers and ReLU activation. We apply two consecutive blocks to every input. Higher-resolution outputs are downsampled and concatenated with the lower resolution inputs before being passed through the next two block. Based on the obtained lowest resolution features, the final relative pose estimation is performed using the same pose prediction head as in [17].

A secondary challenge arises when training supervised and self-supervised tasks simultaneously. Some self-supervised tasks, such as 3D scene flow estimation and motion mask segmentation, struggle to converge when trained alongside the three supervised segmentation tasks using a single shared encoder. It is possible that the gradients from the supervised tasks are sufficiently strong to overshadow those from the self-supervised tasks, hindering their convergence.

To address this issue, we adopt a knowledge distillation strategy. We first train a teacher model consisting of three encoders and five decoders similar to [18]: one Swin encoder for depth estimation and the three supervised segmentation tasks, one ResNet18 encoder for pose estimation, and one ResNet18 encoder for 3D scene flow and motion mask segmentation. We then use the encoder-decoder pair responsible for 3D scene flow and motion mask segmentation in the teacher model to supervise these two tasks in the unified encoder model. The associated distillation loss is defined as:

$$\mathbf{L}_{\text{distil}} = \beta_1 \cdot \|\mathbf{F}_{C_{\text{teacher}}} - \mathbf{F}_{C_{\text{student}}}\|_1 + \beta_2 \cdot \|\mathbf{M}_{\text{teacher}} - \mathbf{M}_{\text{student}}\|_1 \quad (3)$$

Finally, we train the entire framework using a weighted sum of the supervised, self-supervised, and distillation losses:

$$\mathbf{L}_{\text{total}} = \lambda_1 \cdot \mathbf{L}_{\text{sup}} + \lambda_2 \cdot \mathbf{L}_{\text{ssup}} + \lambda_3 \cdot \mathbf{L}_{\text{distil}} \quad (4)$$

D. Efficient Steering Estimation from Dense Latent Space

For the steering command, we used the pre-trained encoder, which was frozen, followed by an attentive pooling mechanism [27] to process the steering input. The encoder’s outputs were fed into the attentive pooler, which takes a sequence of 16 images to compute the steering angle. This approach effectively used the encoder’s latent representations while applying steering-specific attention through the pooling mechanism. During training, we optimized the loss L_{pred} , which is defined as follows:

$$L_{\text{pred}} = \sum_i w_i (\hat{\mathbf{y}}^{(i)} - \mathbf{y}^{(i)})^2 / \sum_i w_i, \quad (5)$$

where $w_i = \exp(\lambda \cdot |\mathbf{y}^{(i)}|)$, with λ representing the factor modulating the influence of the steering command’s magnitude, $|\mathbf{y}^{(i)}|$, on the loss. To evaluate the model’s performance, we employed the mean squared error (MSE) metric.



Fig. 3: Qualitative results. Left to right: Input, panoptic, instance, semantic output, depth, motion mask, independant flow.

IV. EXPERIMENTAL RESULTS

A. Training Setup

We use the KITTI Eigen split for initial ablation and CityScapes for the remaining experiments, with image resolutions of 192×640 and 192×512 , respectively. Images are preprocessed into triples using scripts from [16]. For CityScapes, the lower 25% of images is cropped to exclude the front car [28]. The entire CityScapes dataset is used for supervised segmentation tasks. Pretraining is conducted on a single NVIDIA RTX A5000 with a batch size of 6 (3 images for segmentation and 3 triples for other tasks) over four steps: (1) training the shared encoder with depth, pose, and segmentation decoders for 60,000 steps, (2) training the 3D scene flow decoder for 40,000 steps with other components frozen, (3) training the pose decoder, 3D scene flow decoder, and motion mask segmentation decoder for 40,000 steps with other components frozen, and (4) training the whole network for 250,000 steps. After pretraining, we follow the tenfold cross-validation procedure by Lechner *et al.* [2] to fine-tune the model on the steering angle estimation task. The values of hyperparameters are: $\lambda_{cls} = 2, \lambda_{bce} = \lambda_{dice} = \lambda_c = 5, \lambda_{contrast} = 0.5, \lambda_m = \lambda_g = \beta_1 = 0.1, \beta_2 = 1e-3, \lambda_1 = \lambda_2 = \lambda_3 = 1$.

B. Ablation Studies

Multi-scale pose decoder. To evaluate the effectiveness of our proposed multi-scale pose decoder, we conducted depth estimation experiments using the KITTI Eigen split dataset. This dataset was selected because accurate depth estimation can be achieved with just a depth and a pose network, allowing us to more clearly isolate and assess the contribution of our multi-scale pose decoder. Table I-1 presents the depth estimation results on the KITTI dataset. Our findings reveal that a naive approach of using a shared encoder—by concatenating the lowest-level features of source and target images and passing them through a pose prediction head—results in a decline in depth estimation performance. This trend is evident in both the Monodepth2 model [17] and our Swin encoder. In contrast, using our multi-scale pose decoder maintains depth performance comparable to using a separate ResNet18 encoder specifically for pose estimation.

Knowledge distillation for 3D flow & motion mask. We evaluate the effectiveness of knowledge distillation in training our shared encoder on the CityScapes dataset, which includes many dynamic objects, making 3D scene flow and motion mask networks crucial. Table I-2 shows the depth error and accuracy for different models. First, using

	Model	MS	FM	KD	Error (\downarrow)		Acc. (\uparrow)
					Abs_{rel}	$RMSE_{log}$	$\delta < 1.25$
1	$MD2_{separate}$				0.115	0.193	0.877
	$MD2_{shared}$				0.125	0.201	0.857
	$Our_{separate}$				0.108	0.183	0.884
	Our_{shared}				0.117	0.190	0.872
	Our_{shared}	✓			0.109	0.184	0.884
2	$Our_{separate}$				0.103	0.157	0.885
	Our_{shared}	✓			0.126	0.182	0.850
	Our_{shared}	✓	✓		0.134	0.183	0.833
	Our_{shared}	✓	✓	✓	0.106	0.158	0.888

TABLE I: **1)** Ablation on multi-scale pose decoder using KITTI dataset. **2)** Analysis on knowledge distillation on CityScapes. MS, FM, and KD refers multi-scale pose decoder, 3D scene Flow & Motion mask, and Knowledge Distillation respectively. For the separate encoder, a ResNet18 was employed similar to [17].

a shared encoder with our multi-scale pose decoder achieves good performance compared to using separate encoders for different tasks. Second, training the shared encoder without knowledge distillation leads to suboptimal performance, even worse than the shared encoder model that doesn't consider 3D scene flow and motion masks. However, incorporating knowledge distillation improves the shared encoder's performance, making its performance inline with models with separate encoders. This highlights the effectiveness of our strategy.

Panoptic, instance, and semantic segmentations. To make a fair comparison, we trained OneFormer using the same batch size as our multi-task model. Table II shows the results for Panoptic Quality (PQ), Average Precision (AP), and Intersection over Union (IoU) respectively for panoptic, instance, and semantic segmentation tasks. We can observe that the segmentation performance of our multi-task model closely matches that of the OneFormer model, confirming the state-of-the-art capability of our approach.

C. Comparison with State-of-the-Art Methods

Since our multi-task model aligns closely with the state-of-the-art OneFormer model for segmentation tasks, we only focus on comparing depth estimation with other leading

	PQ (\uparrow)	AP (\uparrow)	IoU (\uparrow)
OneFormer [14]	55.8	28.4	74.3
Our multi-task model	56.0	28.6	74.2

TABLE II: Ablation study on panoptic, instance, and semantic segmentation tasks.

Method	IM	Semantics	# <i>f</i> at inference	D	Error metric (↓)				Accuracy metric (↑)		
					<i>Abs_{rel}</i>	<i>Sq_{rel}</i>	<i>RMSE</i>	<i>RMSE_{log}</i>	$\delta < 1.25$	$\delta < 1.25^2$	$\delta < 1.25^3$
Monodepth2 [17]			1	K	0.115	0.903	4.863	0.193	0.877	0.959	0.981
LiteMono [29]			1	K	0.101	0.729	4.454	0.178	0.897	0.965	0.983
Struct2Depth [30]	✓	✓	1	K	0.141	1.026	5.290	0.215	0.816	0.945	0.979
RM-Depth [31]	✓		1	K	0.107	0.687	4.476	0.181	0.883	0.964	0.984
Dynamo-Depth [18]	✓		1	K	0.112	0.758	4.505	0.183	0.873	0.959	0.984
Ours (wo 3D scene flow)			<u>1</u>	K	<u>0.109</u>	<u>0.818</u>	<u>4.654</u>	<u>0.184</u>	<u>0.884</u>	<u>0.963</u>	<u>0.983</u>
Struct2Depth [30]	✓	✓	1	CS	0.145	1.737	7.280	0.205	0.813	0.942	0.978
Li <i>et al.</i> [32]	✓	✓	1	CS	0.119	1.290	6.980	0.190	0.846	0.952	0.982
RM-Depth [31]	✓		1	CS	0.100	0.839	5.774	0.154	0.895	0.976	0.993
Zhong <i>et al.</i> [33]	✓		2	CS	0.098	0.946	5.553	0.148	0.908	0.977	0.992
ManyDepth [28]	✓		2	CS	0.114	1.193	6.223	0.170	0.875	0.967	0.989
Ours	✓	✓	<u>1</u>	CS	<u>0.106</u>	<u>1.033</u>	<u>5.913</u>	<u>0.158</u>	<u>0.888</u>	<u>0.974</u>	<u>0.982</u>

TABLE III: Depth evaluation on the KITTI (K), and CityScapes (CS) Dataset. IM stands for independent motion. #*f* indicates the number of frames during inference. D is the used dataset for training and evaluation. **Bold** is best. Underline is ours.

methods. Table III presents depth estimation results on the KITTI and CityScapes datasets.

On KITTI, due to the lack of labeled segmentation data, our model is trained without supervision but still surpasses the average performance of state-of-the-art methods. Notably, it outperforms several established methods (*e.g.*, Struct2Depth) across all metrics, even without independent motion and segmentation support. Similarly, on CityScapes, our model shows competitive results, performing better than some methods and approaching the best results for each metric. It is important to highlight that most other methods rely on off-the-shelf segmentation models or use multiple encoders for pose and/or motion estimation.

Finally, Figure 3 shows qualitative results of our multi-task model. The panoptic, instance, and semantic segmentation demonstrate high quality, consistent with the strong quantitative results. Additionally, the quality of the estimated flow and motion mask demonstrate the contribution of these outputs to improved depth estimation compared to the model without the 3D scene flow and motion mask network.

D. From Dense Latent Space to Steering Angle: Evaluation

Table IV showcases the performance of various models for steering prediction, including our proposed Swin-AttnPool approach and several existing CNN-based [2] and VAE-based models [5]. While our model shows higher training and test errors compared to some of the baseline models, it is important to note that our approach is training the decision module with direct latent space from frozen encoder and aims to leverage a more comprehensive and human-like understanding of the real driving environment.

Model	Training error	Test error
CNN-GRU (64 units)	1.25 ± 1.02	5.06 ± 6.64
CNN-LSTM (64 units)	0.19 ± 0.05	3.17 ± 3.85
VAE-LSTM (64 units)	0.54 ± 0.26	4.70 ± 4.80
VAE-LSTM (19 units)	0.60 ± 0.30	6.75 ± 8.33
<u>Swin-AttnPool (Ours)</u>	<u>3.20 ± 1.50</u>	<u>6.15 ± 4.86</u>

TABLE IV: Results from the passive lane-keeping evaluation across tenfold cross-testing. **Bold** is best. Underline is ours.

V. DISCUSSION AND CONCLUSION

Training all tasks within a single encoder using a naive approach often leads to sub-optimal performance for some tasks. Our method is one of the first attempts to incorporate more human-like perception information into a shared encoder, achieving performance comparable to multi-encoder methods in the literature.

We argue that accurate driving requires human-like perception and decision-making. To enhance the decision-making model, we propose using a dense feature space enriched with human-understandable features or those that can infer such features. While this approach may show higher numerical errors in certain evaluations, it could offer a richer and more contextual understanding of the driving scene, leading to more robust and interpretable decisions in complex real-world scenarios. The higher errors may result from the model learning to consider a broader range of factors beyond just lane-keeping, which could ultimately benefit overall driving performance but is not fully reflected by the current metric.

In terms of conclusion, we presented in this work a unified encoder achieved through multi-task learning for autonomous driving, leveraging human-like visual perception needed for navigation. By integrating knowledge from critical computer vision tasks such as depth, pose, 3D scene flow estimation, and various segmentation tasks into a single encoder, our approach allows efficient and compact multi-task inference. We addressed key challenges in multi-task training in ensuring the efficiency on each task. First, we introduce a novel multi-scale pose decoder to better estimate the relative pose between frames and improve the depth performance on scenes with few dynamic objects such as KITTI. Second, we propose to apply knowledge distillation from a multi-encoder model pretrained on the same tasks to stabilize the training process. Our experimental results demonstrate that the performance on individual tasks is competitive with state-of-the-art methods within a single encoder. Finally, when directly leveraging latent space from the unified encoder, such architecture is able to achieve coherent steering angle estimation by incorporating diverse encoded visual information for robust autonomous navigation.

REFERENCES

- [1] C. Chen, A. Seff, A. Kornhauser, and J. Xiao, "Deepdriving: Learning affordance for direct perception in autonomous driving," in *2015 IEEE International Conference on Computer Vision (ICCV)*, 2015, pp. 2722–2730.
- [2] M. Lechner, R. Hasani, A. Amini, T. Henzinger, D. Rus, and R. Grosu, "Neural circuit policies enabling auditable autonomy," *Nature Machine Intelligence*, vol. 2, pp. 642–652, 2020.
- [3] J. Kim and J. Canny, "Interpretable learning for self-driving cars by visualizing causal attention," in *2017 IEEE International Conference on Computer Vision (ICCV)*, 2017, pp. 2961–2969.
- [4] H. Xu, Y. Gao, F. Yu, and T. Darrell, "End-to-end learning of driving models from large-scale video datasets," in *2017 IEEE Conference on Computer Vision and Pattern Recognition (CVPR)*, 2017, pp. 3530–3538.
- [5] A. Bairouk, M. Maras, S. Herlin, A. Amini, M. Blanchon, R. Hasani *et al.*, "Exploring latent pathways: Enhancing the interpretability of autonomous driving with a variational autoencoder," *arXiv preprint arXiv:2404.01750*, 2024.
- [6] V. Rausch, A. Hansen, E. Solowjow, C. Liu, E. Kreuzer, and J. Hedrick, "Learning a deep neural net policy for end-to-end control of autonomous vehicles," in *2017 American Control Conference (ACC)*, 2017, pp. 4914–4919.
- [7] S. Sharma, G. Tewolde, and J. Kwon, "Behavioral cloning for lateral motion control of autonomous vehicles using deep learning," in *2018 IEEE International Conference on Electro/Information Technology (EIT)*, 2018, pp. 490–495.
- [8] M. Bojarski, D. Del Testa, D. Dworakowski, B. Firner, B. Flepp, P. Goyal *et al.*, "End to end learning for self-driving cars," *arXiv preprint arXiv:1604.07316*, 2016.
- [9] T.-D. Do, M.-T. Duong, Q.-V. Dang, and M.-H. Le, "Real-time self-driving car navigation using deep neural network," in *2018 4th International Conference on Green Technology and Sustainable Development (GTSD)*, 2018, pp. 7–12.
- [10] M. Bojarski, P. Yeres, A. Choromańska, K. Choromański, B. Firner, L. Jackel, and U. Muller, "Explaining how a deep neural network trained with end-to-end learning steers a car," *arXiv preprint arXiv:1704.07911*, vol. abs/1704.07911, 2017.
- [11] L. Capito, U. Ozguner, and K. Redmill, "Optical flow based visual potential field for autonomous driving," in *2020 IEEE Intelligent Vehicles Symposium (IV)*, 2020, pp. 885–891.
- [12] A. Majid, S. Kausar, S. Tehsin, and A. Jameel, "A fast panoptic segmentation network for self-driving scene understanding," *Computer Systems Science & Engineering*, vol. 43, no. 1, 2022.
- [13] A. Kirillov, K. He, R. Girshick, C. Rother, and P. Dollár, "Panoptic segmentation," in *Proceedings of the IEEE/CVF Conference on Computer Vision and Pattern Recognition*, 2019, pp. 9404–9413.
- [14] J. Jain, J. Li, M. Chiu, A. Hassani, N. Orlov, and H. Shi, "Oneformer: One transformer to rule universal image segmentation," in *2023 IEEE/CVF Conference on Computer Vision and Pattern Recognition (CVPR)*, 2023, pp. 2989–2998.
- [15] A. Bhoi, "Monocular depth estimation: A survey," *arXiv preprint arXiv:1901.09402*, 2019.
- [16] T. Zhou, M. Brown, N. Snavely, and D. Lowe, "Unsupervised learning of depth and ego-motion from video," in *Proceedings of the IEEE Conference on Computer Vision and Pattern Recognition (CVPR)*, 2017, pp. 1851–1858.
- [17] C. Godard, O. Mac Aodha, M. Firman, and G. J. Brostow, "Digging into self-supervised monocular depth estimation," in *Proceedings of the IEEE/CVF International Conference on Computer Vision*, 2019, pp. 3828–3838.
- [18] Y. Sun and B. Hariharan, "Dynamo-depth: Fixing unsupervised depth estimation for dynamical scenes," *arXiv preprint arXiv:2310.18887*, vol. abs/2310.18887, 2023.
- [19] J. Hur and S. Roth, "Self-supervised monocular scene flow estimation," in *Proceedings of the IEEE/CVF Conference on Computer Vision and Pattern Recognition*, 2020, pp. 7396–7405.
- [20] —, "Self-supervised multi-frame monocular scene flow," in *Proceedings of the IEEE/CVF Conference on Computer Vision and Pattern Recognition*, 2021, pp. 2684–2694.
- [21] Y. Jiao, T. Tran, and G. Shi, "Effiscene: Efficient per-pixel rigidity inference for unsupervised joint learning of optical flow, depth, camera pose and motion segmentation," in *2021 IEEE/CVF Conference on Computer Vision and Pattern Recognition (CVPR)*, 2021, pp. 5534–5543.
- [22] H. M. Eraqi, M. N. Moustafa, and J. Honer, "End-to-end deep learning for steering autonomous vehicles considering temporal dependencies," *arXiv preprint arXiv:1710.03804*, 2017.
- [23] H. Xu, Y. Gao, F. Yu, and T. Darrell, "End-to-end learning of driving models from large-scale video datasets," in *Proceedings of the IEEE Conference on Computer Vision and Pattern Recognition*, 2017, pp. 2174–2182.
- [24] Z. Liu, Y. Lin, Y. Cao, H. Hu, Y. Wei, Z. Zhang *et al.*, "Swin transformer: Hierarchical vision transformer using shifted windows," in *Proceedings of the IEEE/CVF International Conference on Computer Vision*, 2021, pp. 10 012–10 022.
- [25] M. Cordts, M. Omran, S. Ramos, T. Rehfeld, M. Enzweiler, R. Benenson *et al.*, "The cityscapes dataset for semantic urban scene understanding," in *Proceedings of the IEEE Conference on Computer Vision and Pattern Recognition*, 2016, pp. 3213–3223.
- [26] D. Han, J. Shin, N. Kim, S. Hwang, and Y. Choi, "Transdssl: Transformer based depth estimation via self-supervised learning," *IEEE Robotics and Automation Letters*, vol. 7, pp. 10 969–10 976, 2022.
- [27] F. Chen, G. Datta, S. Kundu, and P. Beerel, "Self-attentive pooling for efficient deep learning," 2022. [Online]. Available: <https://arxiv.org/abs/2209.07659>
- [28] J. Watson, O. Mac Aodha, V. Prisacariu, G. Brostow, and M. Firman, "The temporal opportunist: Self-supervised multi-frame monocular depth," in *Proceedings of the IEEE/CVF Conference on Computer Vision and Pattern Recognition*, 2021, pp. 1164–1174.
- [29] N. Zhang, F. Nex, G. Vosselman, and N. Kerle, "Lite-mono: A lightweight cnn and transformer architecture for self-supervised monocular depth estimation," in *Proceedings of the IEEE/CVF Conference on Computer Vision and Pattern Recognition*, 2023, pp. 18 537–18 546.
- [30] V. Casser, S. Pirk, R. Mahjourian, and A. Angelova, "Depth prediction without the sensors: Leveraging structure for unsupervised learning from monocular videos," in *Proceedings of the AAAI Conference on Artificial Intelligence*, vol. 33, no. 01, July 2019, pp. 8001–8008.
- [31] T. W. Hui, "Rm-depth: Unsupervised learning of recurrent monocular depth in dynamic scenes," in *Proceedings of the IEEE/CVF Conference on Computer Vision and Pattern Recognition*, 2022, pp. 1675–1684.
- [32] H. Li, A. Gordon, H. Zhao, V. Casser, and A. Angelova, "Unsupervised monocular depth learning in dynamic scenes," in *Conference on Robot Learning*. PMLR, October 2021, pp. 1908–1917.
- [33] J. Zhong, X. Huang, and X. Yu, "Multi-frame self-supervised depth estimation with multi-scale feature fusion in dynamic scenes," in *Proceedings of the 31st ACM International Conference on Multimedia*, 2023, pp. 2553–2563.